Front. Struct. Civ. Eng. 2021, 15(3): 576–594
https://doi.org/10.1007/s11709-021-0728-6

RESEARCH ARTICLE

Fatigue shear performance of concrete beams reinforced with hybrid (glass-fiber-reinforced polymer + steel) rebars and stirrups

Peng ZHU[a], Jiajing XU[b], Wenjun QU[a*]

[a] *Department of Structural Engineering, Tongji University, Shanghai 200092, China*

[b] *School of Transportation and Civil Engineering, Nantong University, Nantong 226019, China*

[*] *Corresponding author. E-mail: quwenjun.tj@tongji.edu.cn*

ABSTRACT Reinforced concrete beams consisting of both steel and glass-fiber-reinforced polymer rebars exhibit excellent strength, serviceability, and durability. However, the fatigue shear performance of such beams is unclear. Therefore, beams with hybrid longitudinal bars and hybrid stirrups were designed, and fatigue shear tests were performed. For specimens that failed by fatigue shear, all the glass-fiber-reinforced polymer stirrups and some steel stirrups fractured at the critical diagonal crack. For the specimen that failed by the static test after 8 million fatigue cycles, the static capacity after fatigue did not significantly decrease compared with the calculated value. The initial fatigue level has a greater influence on the crack development and fatigue life than the fatigue level in the later phase. The fatigue strength of the glass-fiber-reinforced polymer stirrups in the specimens was considerably lower than that of the axial tension tests on the glass-fiber-reinforced polymer bar in air and beam-hinge tests on the glass-fiber-reinforced polymer bar, and the failure modes were different. Glass-fiber-reinforced polymer stirrups were subjected to fatigue tension and shear, and failed owing to shear.

KEYWORDS fatigue, shear, hybrid stirrups, hybrid reinforcement, fiber-reinforced polymer

1 Introduction

Steel corrosion is a major problem in steel-reinforced concrete (SRC) structures. Fiber-reinforced polymer (FRP) bars are used as substitutes for steel bars as they are noncorrosive, possess high strength, and are light. However, the disadvantages of FRP reinforcement, including low ductility and elastic modulus, result in FRP-reinforced concrete (FRPRC) structures with large deflections and crack widths. A hybrid system combining FRP rebars with steel rebars was developed [1]. This hybrid system possesses improved serviceability compared with pure FRPRC systems and better durability than SRC systems [2–4]. As for the static performance, results by Newhook [5] showed that the ductility is ensured by the steel yielding, and the capacity increases owing to the strength of the glass-fiber-reinforced polymer (GFRP). Aiello and Ombres [2] conducted experiments on beams with aramid-fiber-reinforced polymer (AFRP) and steel rebars. It was concluded that the deflection under service conditions and crack width of the hybrid reinforced concrete (RC) beams were smaller than those of the FRPRC beams were. Qu et al. [3] studied the influences of the reinforcement amount and ratio of GFRP to steel on hybrid RC beams through eight tests. Hybrid elements presented high strength, acceptable serviceability and ductility. In addition, a prediction model was developed for the flexural behavior of the hybrid system. Beams with pure steel bars, pure GFRP bars, and hybrid bars were compared, where hybrid RC beams showed higher ductility than pure GFRP reinforced beams did [6]. The reinforcement ratio and area ratio of FRP to steel bars (A_f/A_s) were proposed to ensure ductile failure, and a new ductility index was introduced [7]. Kara et al. [8]

Article history: Received Oct 29, 2020; Accepted Jan 22, 2021

developed a numerical method to calculate the flexural capacity, curvature, and deflection of hybrid RC beams based on sectional analysis. Bencardino et al. [9] presented a 2D finite element model considering tension stiffening. Zhu et al. [10] investigated the fatigue flexural behaviors of RC beams with both GFRP and steel bars through experiments and proposed theories to predict the deformation of GFRP- and steel-reinforced beams under fatigue. Xu et al. [11] developed an analytical model to predict the strain development for hybrid RC beams under fatigue, and the residual strains were considered. Li et al. [12] studied the fatigue behavior of sea sand concrete beams with basalt-fiber-reinforced polymer (BFRP) bars, and the test parameters were the load levels and specimen sizes. It was proposed that 0.55 F_u was a threshold. Zhao et al. [13] tested 13 concrete beams with GFRP and carbon-fiber-reinforced polymer (CFRP) bars under static or fatigue loading after exposure to different temperatures. The GFRP RC beams exhibited a shorter fatigue life than the CFRP RC beams when the elevated temperature was below 400°C.

Considering that the outer stirrups are closer to the outer concrete surface than the longitudinal bars, and thus are more susceptible to severe environments, it is promising to replace steel stirrups with noncorrodible FRPs. Considering the low ductility and elastic modulus of FRPs, a combination of GFRP and steel stirrups was developed with GFRP stirrups at the outer section and steel stirrups inside, and theories for the shear capacity of hybrid RC beams were developed by Zhang [14]. Pang [15] studied the static shear performance of concrete beams with hybrid steel and GFRP stirrups and found that steel stirrups yielding caused failure with crushing of concrete, while no GFRP stirrups fractured. However, the fatigue shear behavior of hybrid GFRP steel RC beams has not been investigated yet.

Studies on the fatigue shear performance of SRC beams with shear reinforcement date back to the 1970s. Ruhnau [16] tested five beams with transverse reinforcement. Repeated loading and overloading can increase stirrup stress. Different web thicknesses were investigated, and a formula to compute the maximum stirrup stress according to the load was proposed. Okamura et al. [17] set the minimum load of 39 kN as a constant in their experiments, and the maximum load varied with a loading frequency of 200 cycles per minute. The main diagonal cracks increased in width and length, whereas new diagonal cracks were observed occasionally. Strains in the stirrups, where diagonal cracks intersected, increased. Furthermore, stress redistribution occurred before any stirrup fracture, and 41 of 42 legs subjected to fracture had the same fracture location. Fracture of the longitudinal bars occurred beside the first fractured stirrup leg. Ueda [18] tested 11 T-beams with shear reinforcement and 16 rectangular beams without shear reinforcement. For T-beams, shear failure occurred with the fracture of stirrups, and it was concluded that the fatigue life increased as the minimum load to maximum load ratio increased. Kwak and Park [19] investigated the fatigue shear performance of high-strength concrete beams. The high-strength beams failed at 57% to 66% of the static ultimate capacity after 2 million cycles, and Teng et al. [20] investigated 12 RC deep beams under fatigue loading. It was concluded that web reinforcements had effects on the fatigue performance of deep beams, and inclined web reinforcements were the most effective. Isojeh et al. [21] tested eight deep beams and found that the fatigue life increased with an increase in longitudinal reinforcement ratios. Strains in the bends of shear reinforcement were lower than those in the longitudinal bars owing to the governing arch mechanism of the deep beams. In this study, fatigue shear behavior of hybrid (GFRP + steel bars and stirrups) RC beams was investigated through laboratory tests.

2 Experimental program

2.1 Specimen design

Three fatigue shear tests (FS-2.54-0.6, FS-2.54-0.4, and FS-2.07-0.4) were designed. The GFRP stirrups were placed outside the steel stirrups to increase their durability. Figure 1 shows the specimen design. The shear span-to-depth ratios (2.54 and 2.07) and the upper limit of fatigue loading (0.4 and 0.6 P_u) were studied. The specimens are named accordingly, e.g., if 2.54 is the shear span-to-depth

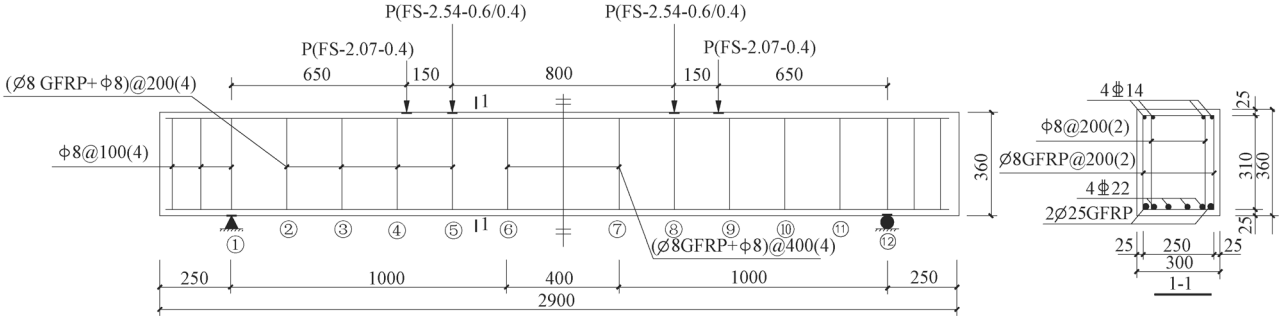

Fig. 1 Specimen dimensions and reinforcement details (note: all dimensions in millimeters; all clear covers = 25 mm).

ratio and 0.6 P_u is the upper limit of fatigue load, the specimen is named as FS-2.54-0.6. The specimens were 2900 mm long, 300 mm wide, and 360 mm high. Four 14-mm longitudinal steel bars were placed at the top and six bars at the bottom, two 25-mm GFRP bars at the corners, and four 22-mm steel bars in the middle. The 8-mm GFRP and steel stirrups were spaced at 400 mm between the loading points. For GFRP stirrups, as shown in Fig. 2, the ratio of internal radius of the bend over diameter is 6.25, which is greater than 3, as required by ACI 440.1R-15 [22]. The tail length is 100 mm, which is greater than 12 times the diameter, as required by ACI 440.1R-15 [22].

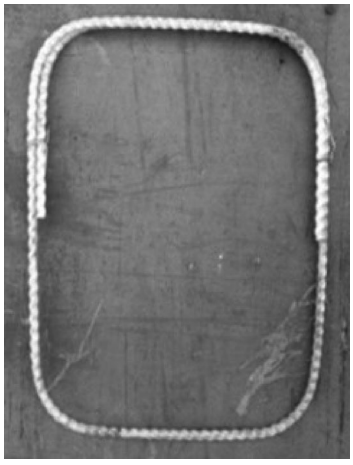

Fig. 2 Photo of GFRP stirrups.

2.2 Materials

For the longitudinal reinforcement, deformed steel bars and GFRP ribbed bars were used, and steel plain bars and GFRP ribbed bars were used as stirrups. GFRP bars with 25-mm diameter were made of E-glass fibers (75% by weight) and vinyl ester resin, and GFRP bars with a diameter of 8 mm were made of E-glass fibers (78% by weight) and epoxy resin. The properties of the reinforcement per GB/T228.1–2010 [23] and GB/T 30022–2013 [24] are listed in Table 1. The proportions of concrete by weight were 1 × 0.66 × 3.22 × 4.27, for cement (PO 52.5), water, sand, and coarse aggregate, respectively. The compressive strength and modulus of elasticity of concrete were 36 and 37720 MPa, respectively, before the beam tests, per GB/T 50081–2002 [25].

2.3 Test setup

Four-point loading tests were performed, and displacements at the mid-span and supports were measured using laser displacement sensors, as shown in Fig. 3. Strain gauges were mounted at one of the GFRP tension bars and one of the steel tension bars, as shown in Fig. 4(a), as well as the stirrups in the loading zone along the expected plane of shear failure, as shown in Figs. 4(b)–4(d). The side of the beam with strain gauges on stirrups is named as "S", and the other side is named as "N".

2.4 Nominal shear strength

In the static tests conducted by Pang [15], shear-compression failure occurred for shear span-to-depth ratios between 2 and 3, and we studied shear span-to-depth ratios of 2.54 and 2.07. The equations for the nominal shear strength of hybrid RC beams were developed by Zhang [14]. Accordingly, the static ultimate load (P_u) was calculated to be 416.4 and 523.2 kN for the designed specimens with shear span-to-depth ratio of 2.54 and 2.07, respectively. The cracking moment (M_{cr}) was determined using the equation for steel RC beams by ACI 318–14 [26], as shown in Eq. (1), where f_r is the modulus of rupture of concrete under static loading, which can be calculated using Eq. (2); I_g is the moment of inertia of the gross section about the centroidal axis, with reinforcement neglected, and h is the overall height of cross section. Accordingly, cracking load (P_{cr}) was calculated to be 60.3 kN for FS-2.54-0.6 and FS-2.54-0.4. In the tests, P_{cr} was 60.9 and 66.9 kN for FS-2.54-0.6 and FS-2.54-0.4, respectively, and the difference between the calculation and test results was 1.0 and 10.9% for FS-2.54-0.6 and FS-2.54-0.4, respectively. The cracking load (P_{cr}) was 74.2 kN for FS-2.07-0.4 and was 83.2 kN in the test; therefore, deviation was 12.1%.

Table 1 Properties of steel and GFRP reinforcement

type	Nominal diameter (mm)	nominal area (mm^2)	immersion area (mm^2)	yield strength (MPa)	ultimate strength (MPa)	modulus of elasticity (GPa)
steel	7.9	49	–	448	579	193
	13.7	147	–	520	641	200
	21.5	363	–	423	570	201
GFRP	7.9	49	55	–	1203	45
	24.5	471	503	–	815	42

Note: The strength and modulus of elasticity were calculated based on the nominal area.

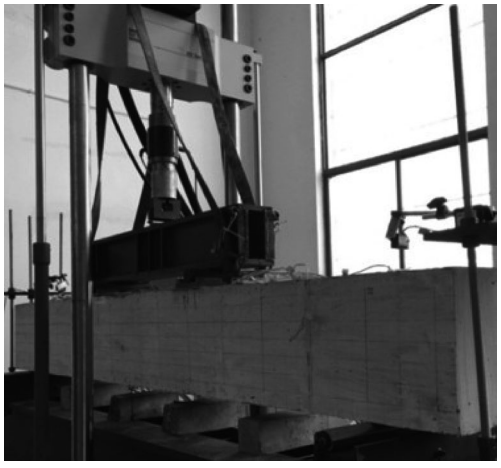

Fig. 3 Test setup.

$$M_{cr} = \frac{2f_r I_g}{h}, \tag{1}$$

$$f_r = 0.62\sqrt{f_c}. \tag{2}$$

2.5 Loading procedures

A static loading test was conducted before fatigue loading and after a predesigned number of fatigue cycles. For the static test, the upper limit of fatigue loading (P_{max}) was applied and then unloaded to 0 kN. The pattern for fatigue loading was a sine wave.

The service load is about 60%–65% of the nominal moment capacity for SRC beams according to Bischoff [27] and about 35% of the ultimate load for FRPRC beams by Alsayed et al. [28] and Rafi et al. [29]. Thus, a value between the service load for the SRC and FRPRC beams was selected as the upper limit of the fatigue loading. For the fatigue load, $0.6P_u$ and $0.4P_u$ were used as the upper limits, and $0.12P_u$ and $0.08P_u$ were used as the lower limits. The ratio of the minimum to maximum load was 0.2, and the same ratio was obtained by Zhang et al. [30]. The fatigue loading was determined, as shown in Table 2. To accelerate the fatigue, the loading frequency for FS-2.54-0.4 and FS-2.07-0.4 was increased from 4 to 6 Hz. The variation in the loading frequency between 1 and 15 Hz had little influence on the fatigue strength as the maximum stress level did not exceed 75% of the static

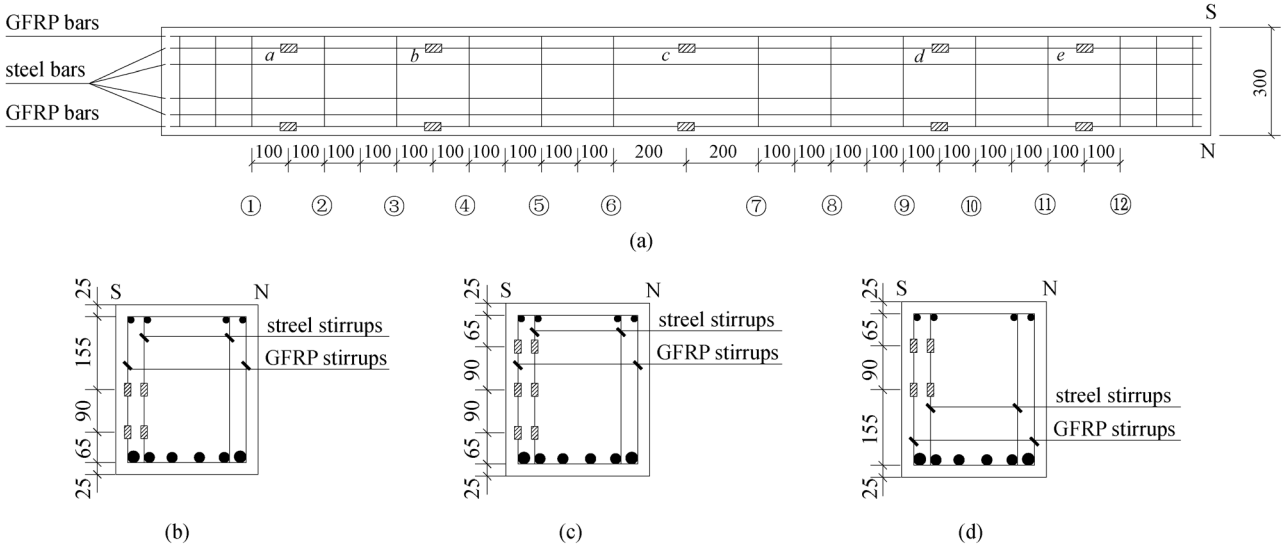

Fig. 4 Strain gauges mounted on GFRP and steel reinforcement: (a) GFRP and steel tension bars at the bottom of the beam; (b) stirrups of #2 and #11; (c) stirrups of #3 and #10; (d) stirrups of #4 and #9.

Table 2 Fatigue loading protocol

specimen	fatigue phase	minimum load P_{min} (kN)	maximum load P_{max} (kN)	frequency (Hz)
FS-2.54-0.6	–	50 ($0.12P_u$)	250 ($0.6P_u$)	4
FS-2.54-0.4	before 2 million cycles	34 ($0.08P_u$)	168 ($0.4P_u$)	6
	2 to 4.5 million cycles	50 ($0.12P_u$)	250 ($0.6P_u$)	
	after 4.5 million cycles	25 ($0.06P_u$)	250 ($0.6P_u$)	
FS-2.07-0.4	before 4 million cycles	42 ($0.08P_u$)	208 ($0.4P_u$)	6
	4 to 4.5 million cycles	50 ($0.10P_u$)	250 ($0.48P_u$)	
	after 4.5 million cycles	25 ($0.05P_u$)	250 ($0.48P_u$)	

strength [31]. For FS-2.54-0.6, an interim static loading test was conducted after 0.01, 0.05, 0.1, and 0.3 million cycles. Similarly, for FS-2.54-0.4, an interim static loading test was conducted after 0.01, 0.05, 0.1, 0.3, 0.5, 1, 2, 3, 4, and 5 million cycles. After 2 million cycles, little damage was observed. The maximum fatigue load was increased to $0.6P_u$ with the minimum load adjusted to $0.12P_u$ accordingly. After 4.5 million cycles, little damage was observed, and the minimum load was reduced to $0.06P_u$, considering that the stress range is one of the significantly important factors influencing fatigue life [31], and a decrease in the minimum load with an intact maximum load can result in a decrease in the fatigue life [18]. The ratio of the minimum to maximum load was 0.1, which was obtained by Ueda [18]. For FS-2.07-0.4, an interim static loading test was conducted after 0.01, 0.05, 0.1, 0.3, 0.5, 1, 2, 4, 4.5, 6.5, and 8 million cycles. After 4 million cycles, little damage was observed, and the maximum fatigue load was increased to $0.48P_u$, the capacity of loading system, with the minimum load adjusted to $0.1P_u$ accordingly. After 4.5 million cycles, the minimum load was reduced to $0.05P_u$. A static test was performed to cause the specimen to fail after 8 million cycles.

3 Results and discussion

3.1 Failure modes

The failure modes of the beams are presented in Fig. 5, and the failure of the stirrups is listed in Table 3. The fatigue life for FS-2.54-0.6 was 405000 cycles. Under the maximum load of the static test before fatigue, the maximum crack width of both sides was 0.05 mm. After 50 thousand cycles, slight concrete peeling occurred at the #10 stirrups. The diagonal crack width developed significantly, and a critical diagonal crack formed, which may have been caused by the fracture of the #10 GFRP stirrup after 30000 cycles and the fracture of the #10 steel stirrup after 50000 cycles. This is discussed in more detail in Section 3.2.1. The crack width of the critical diagonal crack on the S and N sides were 0.9 and 0.75 mm, respectively, and the maximum width of other cracks was 0.25 mm. After 300000 cycles, the crack width of the critical diagonal crack was 1.45 mm at the #10 stirrups, and the maximum width of the other cracks was 0.3 mm. As shown in Fig. 6(a), the three GFRP stirrups fractured at the critical diagonal crack. The fracture surfaces of the GFRP stirrups were smooth, unlike broomlike failure, typically in static tensile tests, and all fractures were located outside the lap part. The two steel stirrups fractured at the critical diagonal crack. The fracture surfaces of #9 steel stirrups were smooth, while those of #10 steel stirrups were rough, and obvious necking was observed. In addition, no longitudinal bars fractured. As the stirrups fractured, the beam failed at the critical diagonal crack, and the angle between the critical diagonal crack and horizontal axis of the beam was approximately 26°, as shown in Fig. 5(a). The concrete in the shear-compression zone was not crushed during failure.

The fatigue life of FS-2.54-0.4 was 5.46 million cycles. Under the maximum load of the static test before fatigue, the maximum crack width was 0.05 mm. After two million cycles, the maximum crack width was 0.15 mm under the maximum load. As the maximum and minimum loads increased after two million cycles, the maximum crack width increased, and diagonal cracks developed toward the loading point. After three million cycles, the critical diagonal crack formed with a width of 0.3 mm, whereas the maximum width of the other cracks was 0.15 mm. After 4.5 million cycles, the minimum load reduced, and the crack width did not change significantly. As shown in Fig. 5(b), the beam failed at the critical diagonal crack, and the angle between the critical diagonal crack and the horizontal axis of the beam was approximately 27°. As shown in Fig. 6(b), the three GFRP stirrups fractured at the critical diagonal crack. The fracture surfaces of the GFRP stirrups were smooth, and all fractures were located outside the lap. Two steel stirrups fractured at the critical diagonal crack. The fracture surfaces of the #9 steel stirrups were smooth, one longitudinal steel bar fractured at the location between the #10 and #11 stirrups with a clear fracture

Table 3 Fracture locations of reinforcement

specimens	fracture location			
	steel stirrups	GFRP stirrups	longitudinal steel bars	longitudinal GFRP bars
FS-2.54-0.6	#9 UB-S #9 U-N #10 M-S #10 M-N	#9 UB-S #9 U-N #10 M-S #10 M-N #11 LB-S #11 LB-N	–	–
FS-2.54-0.4	#9 UB-S #9 UB-N #11 LB-S	#9 UB-S #9 U-N #10 M-S #10 M-N #11 LB-S #11 LB-N	location between #10 and #11	–
FS-2.07-0.4	–	#9 T #10 M-S #10 M-N #11 LB-N	–	–

Notes: UB: upper bent portion; U: upper portion of vertical leg; LB: lower bent portion; M: middle part of the vertical leg; T: top horizontal leg; S: the side of the beam where strain in the stirrup is monitored with strain gauges; N: the other side of the beam.

(a)

(b)

(c)

Fig. 5 Failure modes of the beams: (a) FS-2.54-0.6; (b) FS-2.54-0.4; (c) FS-2.07-0.4.

surface. The concrete in the shear-compression zone was not crushed during failure.

FS-2.07-0.4 did not fail after eight million cycles and failed by static loading. In the first four million cycles, the maximum load was low, and the deflection and crack widths were small. The maximum crack width was 0.2 mm under the maximum load. After four million cycles, the maximum and minimum loads increased, and thus the mid-span deflection and the maximum crack width increased. After 4.5 million cycles, the maximum crack width was 0.3 mm. After 6.5 million cycles, the critical diagonal crack formed with a width of 0.4 mm, and the maximum

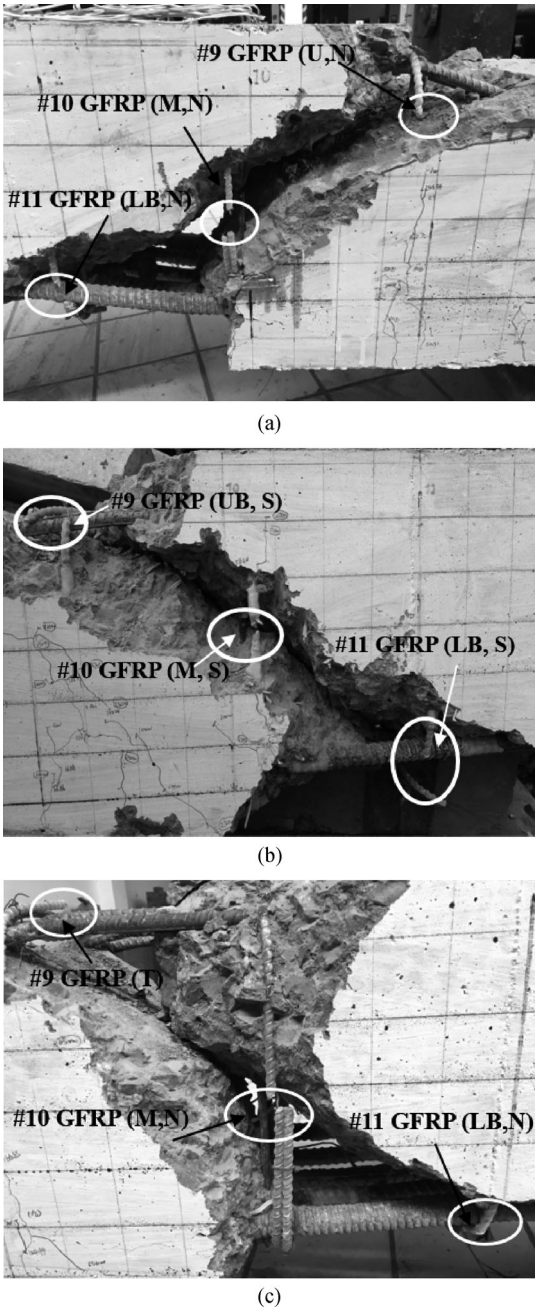

Fig. 6 Reinforcement fracture in three beams (a) FS-2.54-0.6; (b) FS-2.54-0.4; (c) FS-2.07-0.4.

width of the other cracks was 0.2 mm. After eight million cycles, the critical diagonal crack formed with a width of 0.65 mm, and the maximum width of other cracks was 0.3 mm. Subsequently, the beam failed under static loading. As shown in Fig. 5(c), the angle between the critical diagonal crack and the horizontal axis of the beam was approximately 31°, and the concrete in the shear-compression zone was crushed. As shown in Fig. 6(c), three GFRP stirrups fractured at the critical diagonal crack, and all fractures were located outside the lap part. The other stirrups and longitudinal bars did not fracture.

For all three specimens, the three GFRP stirrups (#9, #10, and #11) crossed by the critical diagonal crack fractured. The fracture locations of the #10 and #11 GFRP stirrups were the same in different specimens, while they were different for the #9 GFRP stirrups in different specimens. For FS-2.54-0.6 and FS-2.54-0.4, the #9 GFRP stirrups fractured at the upper bent portion on the S side and the upper portion of the vertical leg on the N side. For FS-2.07-0.4, the #9 GFRP stirrup fractured in the middle of the top horizontal leg by static loading after eight million cycles. In the static shear tests of hybrid reinforced beams conducted by Pang [15], the concrete in the shear-compression zone was crushed with no stirrups fractured. For FS-2.07-0.4, certain damage had accumulated in the stirrups after eight million cycles, and the #9 GFRP stirrup fractured owing to increased compression in the loading zone in the static test. Stirrups were broken at the corners because of the stress concentration at the contact between the stirrups and longitudinal bars. Stirrups fractured in the nonbent portion of the vertical legs because the tension and shear stress in the stirrups increased as the diagonal cracks crossed through. All fractures of stirrups located outside the lap part, which indicated that the overlap length by ACI 440.1R-15 [22] was sufficient for beams under fatigue loading.

3.2 Strain development in stirrups

3.2.1 Specimen FS-2.54-0.6

As shown in Fig. 7, the strain in different stirrups under the upper limit of the fatigue load developed with fatigue cycles. At the beginning of the fatigue (first 10000 cycles), the strain in the steel stirrups and GFRP stirrups increased rapidly, while that of the #2 GFRP stirrup decreased slightly. With the increase in fatigue cycles, the stirrup strain increased, and at the end of the fatigue life, the strain in some stirrups increased significantly. The strain in the steel and GFRP stirrups at the same location was varied, and the strain in the stirrups varied with height.

Diagonal cracks crossed through the #3 and #4 stirrups, and not through the #2 stirrup, resulting in a small strain in the #2 stirrups during the entire fatigue life. As the #2 stirrups were close to the bearing, they were in compression during the initial stage of fatigue. The strain at the middle height of the #10 GFRP stirrup increased to 5810 με after 30000 cycles, and then the strain dropped sharply to 2126 με at 50000 cycles. The strain in the upper and lower portions of the vertical leg of the #10 GFRP stirrup also reached a peak after 30000 cycles, and then decreased, indicating that the #10 GFRP stirrup may be broken. The strain at the middle height of the #10 steel stirrup increased from 1994 με at 30000 cycles to 6928 με at 52000 cycles, and the strain in the upper portions of the vertical leg of the

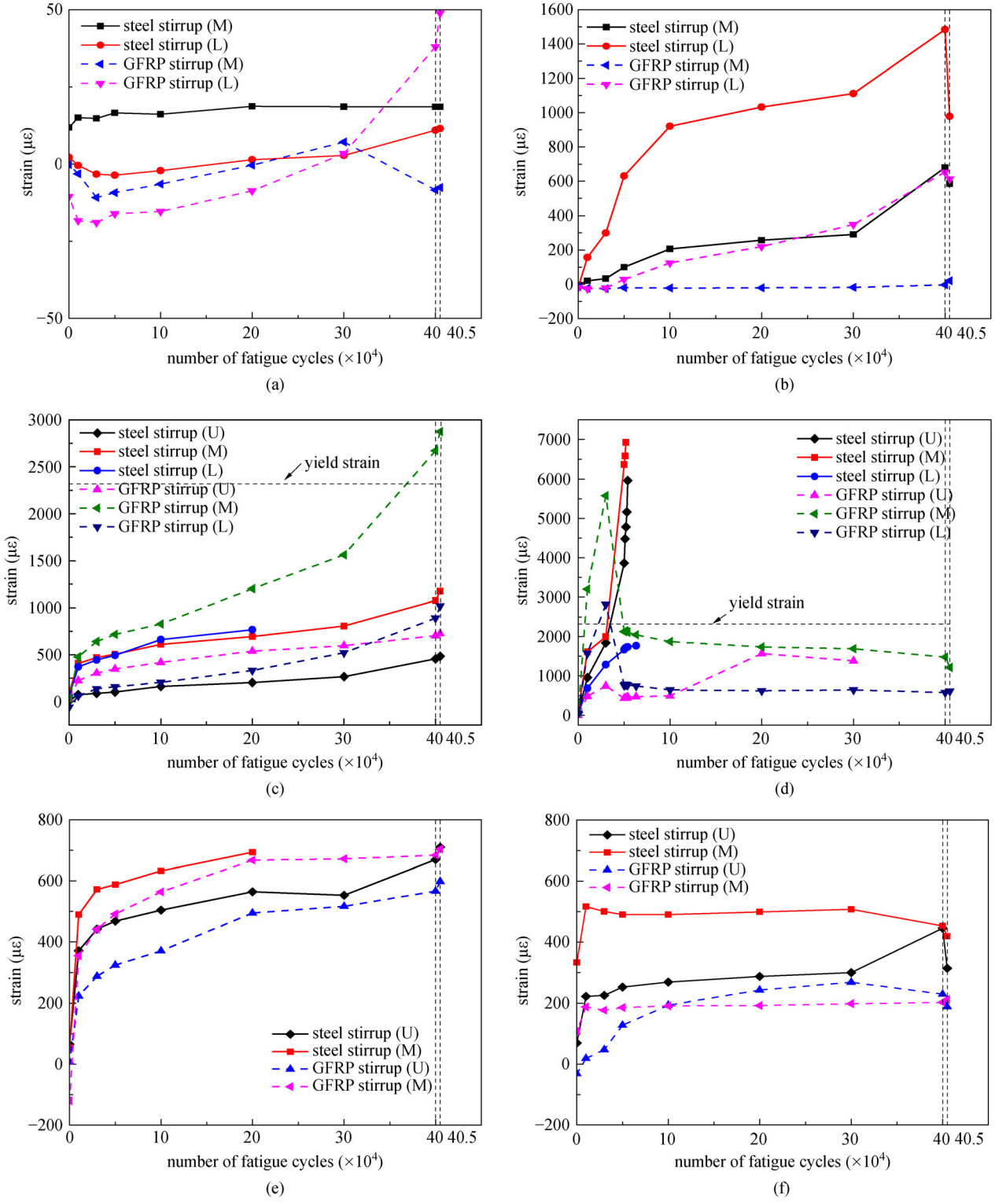

Fig. 7 Strain development in stirrups with fatigue cycles under the upper limit of the fatigue load (FS-2.54-0.6): (a) #2 stirrups; (b) #11 stirrups; (c) #3 stirrups; (d) #10 stirrups; (e) #4 stirrups; (f) #9 stirrups.

#10 steel stirrup increased from 1839 με at 30000 cycles to 5963 με at 54000 cycles. The strain is greater than that of the yielding strain. At 50000 cycles, the residual strain at the middle height of the #10 GFRP and #10 steel stirrups was 1615 and 4313 με, respectively, and yielding and necking of #10 steel stirrups were observed. The strain in

the lower portions of the vertical leg of the #11 GFRP and #11 steel stirrups also increased significantly after 30000 cycles. Therefore, the shear in the #10 GFRP stirrup was transferred to the #10 steel stirrup and #11 stirrup after the #10 GFRP stirrups fractured. Strain gauges at the middle height, upper, and lower portions of the vertical leg of the #10 steel stirrup failed after 52000, 54000, and 63000 cycles, respectively.

The strain at the middle height of the #10 stirrup and that at the lower portion of the vertical leg of the #11 stirrup were greater than that of other heights of the same stirrups, indicating that the stirrup strain through which the critical diagonal crack crossed was greater than that of the other portions of the stirrups. The strains in the #4 and #9 stirrups did not comply with this feature. Stirrups #4 and #9 were close to the constant moment region, and vertical cracks developed from the beam bottom to 135 mm from the top of the #4 stirrup and 110 mm from the top at the #9 stirrups. Thus, strains at the middle height of the #4 and #9 stirrups were greater than those in the other portions. After 405000 cycles, the strains in the #9, #10, and #11 stirrups decreased at locations where the critical diagonal crack crossed through, owing to stress release after the fracture of the stirrups. Meanwhile, the strains in the #2, #3, and #4 stirrups increased owing to the fracture of the #9, #10, and #11 stirrups.

3.2.2 Specimen FS-2.54-0.4

Figure 8 indicates that the strain in different stirrups under the upper limit of the fatigue load developed with fatigue cycles. In the first two million cycles, the strains in the steel and GFRP stirrups were small (steel stirrups: –11–123 με; GFRP stirrups: –91–206 με). The strain in some GFRP stirrups decreased with fatigue cycles, which may have been caused by crack development. After two million cycles, strain gauges at the lower portion of the vertical legs of #3 steel stirrup, those at the top portion and the middle height of the vertical leg of the #4 steel stirrup and that at the top portion of the vertical leg of the #10 steel stirrup failed. From 2 to 2.5 million cycles, the strain in the stirrups increased significantly owing to the increased maximum load. From 2.5 to 4.5 million cycles, strain increased in the stirrups slowed down. The strain at the lower portion of the vertical leg of #11 steel stirrup was 2324 με at 2.02 million cycles when the yield strain was reached. Furthermore, it increased dramatically to 5530, 6512, and 9300 με at 2.05, 2.10, and 2.50 million cycles, respectively, when the steel stirrups were stretched severely. After 4.70 million cycles, the strain increased to hundreds of thousands of micro-strain, and then decreased dramatically to approximately 4000 με. The strain at the lower portion of the vertical leg of the #10 steel stirrup increased to tens of thousands of micro-strain, and then the strain gauge failed. Therefore, the #11 steel stirrup fractured at the lower portion of the vertical leg after 4.70 million cycles, and the shear afforded by the #11 steel stirrup was transferred to nearby stirrups; thus, the strain at the lower portion of the vertical leg of the #10 steel stirrup increased significantly. After 3.0 million cycles, the strain at the middle height of the vertical leg of #3 steel stirrup was close to the yield strain, and the strain gauge failed. After 3.2 million cycles, the yield strain was reached at the middle height of the vertical leg of the #10 steel stirrup, and the strain gauge failed. The strain in the #4 stirrups was significantly larger than that of the #9 stirrup because of the vertical crack developed at the #4 stirrups.

3.2.3 Specimen FS-2.07-0.4

Figure 9 shows that the strain in different stirrups under the upper limit of the fatigue load developed with fatigue cycles. In the first four million cycles, the strains in the steel stirrups and GFRP stirrups were small (steel stirrups: –98–452 με; GFRP stirrups: –85–718 με). In the initial phase of fatigue, all GFRP stirrups were under compression, while all steel stirrups were in tension, except for the top portion of the vertical leg of the #9 steel stirrup, which experienced compressive strain. This is likely because the diagonal crack was still small, the crack width at the outside was smaller than that of the inside, and the GFRP stirrups were placed outside the steel stirrups. After four million cycles, the strain in the #4 stirrups changed slightly, while the strain in the other stirrups increased significantly as the maximum load increased. After 4.5 million cycles, the minimum load decreased, whereas the maximum load remaining unchanged. The strain at the top portion and the middle height of the vertical leg of the #10 steel stirrup decreased, while the other strain measured increased, except for the strain gauges at the middle height of the vertical leg of the #10 GFRP stirrup and at the lower portion of the vertical legs of the #10 steel stirrup. None of the steel stirrups that were measured yielded.

3.3 Stress range in stirrups

3.3.1 Specimen FS-2.54-0.6

The stress range in the steel and GFRP stirrups developed with fatigue cycles, as shown in Fig. 10. Figure 7(a) shows that the strains in the #2 stirrups were low (–25–50 με) during the entire fatigue life and were not analyzed. The stress range was calculated according to the maximum and minimum strains collected at the same location of the stirrups. For steel, the fatigue elastic modulus was 5% lower than the static value [32]. To calculate the fatigue elastic modulus of the GFRP, Eq. (3) was proposed by Noël and Soudki [33], where E_0 is the initial elastic modulus, σ_e is the applied effective stress range, N is the number of applied cycles, and E_f is the fatigue

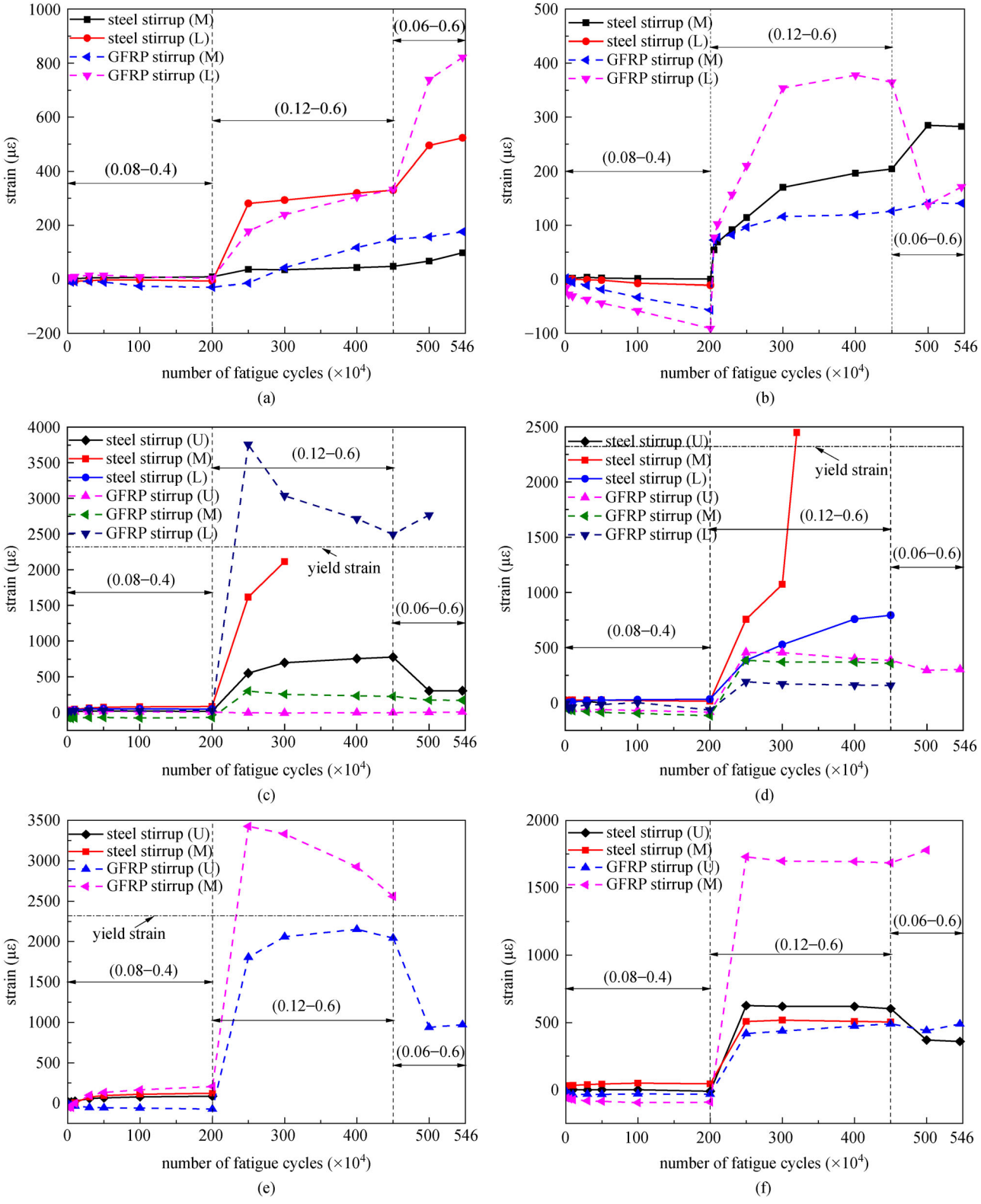

Fig. 8 Strain development in stirrups with fatigue cycles under the upper limit of the fatigue load (FS-2.54-0.4): (a) #2 stirrups; (b) #11 stirrups; (c) #3 stirrups; (d) #10 stirrups; (e) #4 stirrups; (f) #9 stirrups. Note: the numbers in brackets in the figures indicate stress levels.

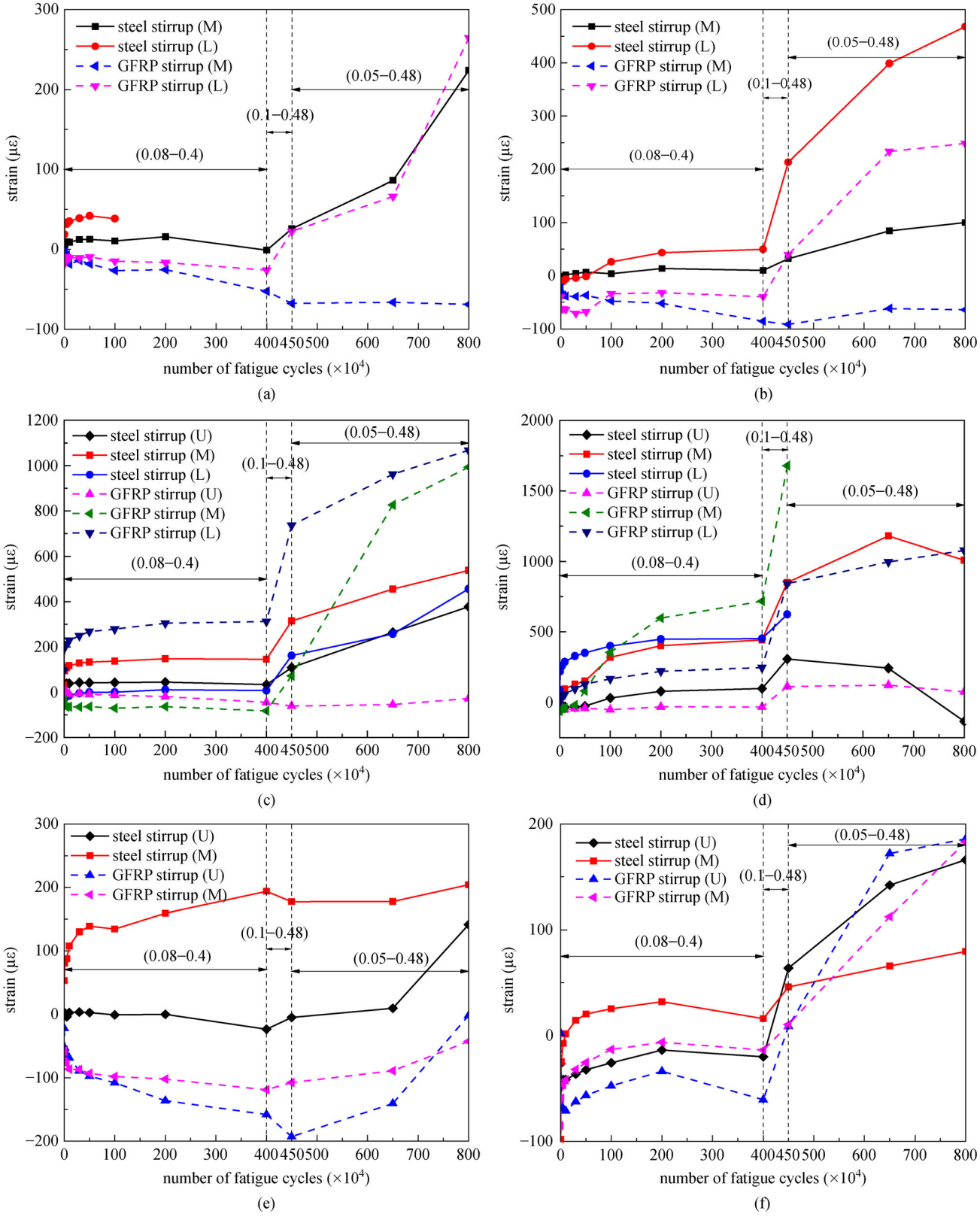

Fig. 9 Strain development in stirrups with fatigue cycles under the upper limit of the fatigue load (FS-2.07-0.4): (a) #2 stirrups; (b) #11 stirrups; (c) #3 stirrups; (d) #10 stirrups; (e) #4 stirrups; (f) #9 stirrups.

elastic modulus. According to the stress range in the GFRP stirrups in Table 4, the calculated fatigue elastic modulus was 99% of the initial value because of the low stress range in the GFRP stirrups. Therefore, the elastic modulus deterioration of the stirrups was not considered. The stress range in the #10 GFRP stirrup reached a maximum at 30000 cycles, as shown in Fig. 10, and then the #10 GFRP stirrup fractured, and the #10 steel stirrups stretched significantly. After 30000 cycles, the stress range in the #11 steel and #3 GFRP stirrups increased significantly with fatigue cycles. GFRP stirrups #9 and #11 fractured under a low stress range during the entire fatigue process, while the #3 GFRP stirrup did not fracture as the stress range increased significantly at 400000 cycles. Consequently, the GFRP stirrups fractured by the fatigue shear, and the tension stress range in the GFRP stirrups did not have significant influence on the fatigue shear life of the specimens.

$$E_{\mathrm{f}} = E_0\left[1 - 1.153 \times 10^{12} N \left(\frac{\sigma_{\mathrm{e}}}{E_0}\right)^{8.062}\right]. \quad (3)$$

3.3.2 Specimen FS-2.54-0.4

Figure 11 shows that the stress range in the steel and GFRP stirrups developed with fatigue cycles. The stress ranges in the steel and GFRP stirrups were low before two million cycles owing to the small stress level. From 2 to 4.5 million cycles, the maximum and minimum fatigue loads increased, and thus the stress range in the stirrups increased. After 4.5 million cycles, the minimum fatigue loads decreased, the stress range in the #2, #3 GFRP stirrups, and the #3 steel stirrup increased, while the stress range in the #9 GFRP stirrups and #9 steel stirrups decreased slightly. The stress ranges in the #9, #10, and #11 GFRP stirrups were lower than those in the #3 and #4 GFRP stirrups, whereas the #9, #10, and #11 GFRP stirrups fractured rather than the #3 and #4 GFRP stirrups. This verified the inference in Section 3.3.1.

3.3.3 Specimen FS-2.07-0.4

Figure 12 shows that the stress range in the steel and GFRP stirrups developed with fatigue cycles and increased with

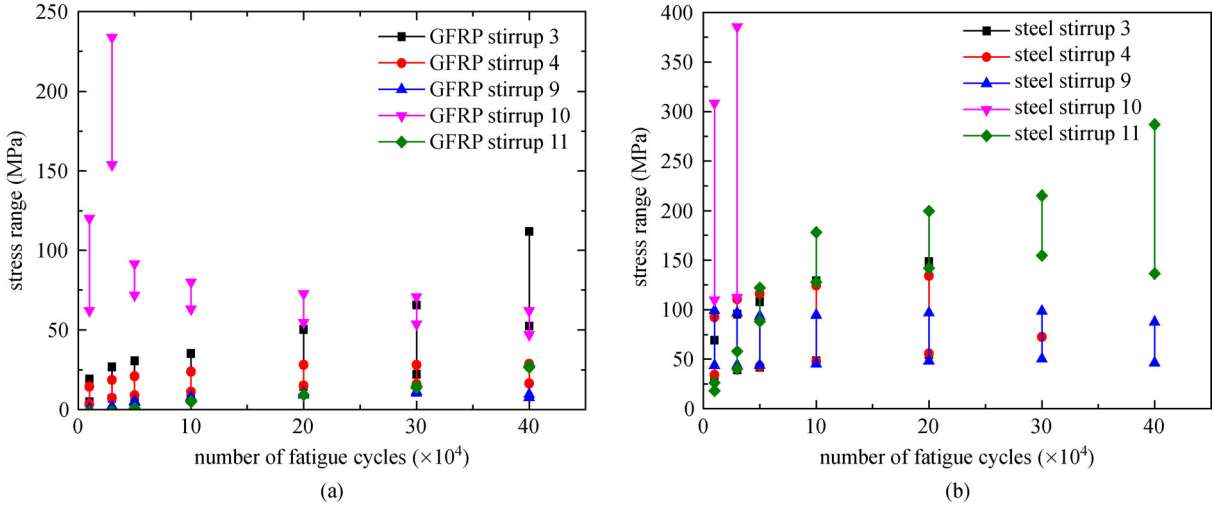

Fig. 10 Stress range in stirrups (FS-2.54-0.6): (a) stress range in GFRP stirrups; (b) stress range in steel stirrups.

Table 4 Maximum stress range in various reinforcements

beam	fatigue phase	maximum stress range in GFRP stirrups (MPa)	maximum stress range in steel stirrups (MPa)	maximum stress range in longitudinal steel bars (MPa)	maximum stress range in longitudinal GFRP bars (MPa)
FS-2.54-0.6	1 cycle	11.3	56.9	175.5	54.9
FS-2.54-0.4	1 cycle	0.5	1.4	97.9	14.7
	2 million cycles	73.0	74.7	220.3	24.7
	4.5 million cycles	93.2	55.8	227.5	22.1
FS-2.07-0.4	1 cycle	3.7	19.7	85.0	30.1
	4 million cycles	12.7	60.2	118.2	41.8
	4.5 million cycles	25.8	79.5	133.9	46.6

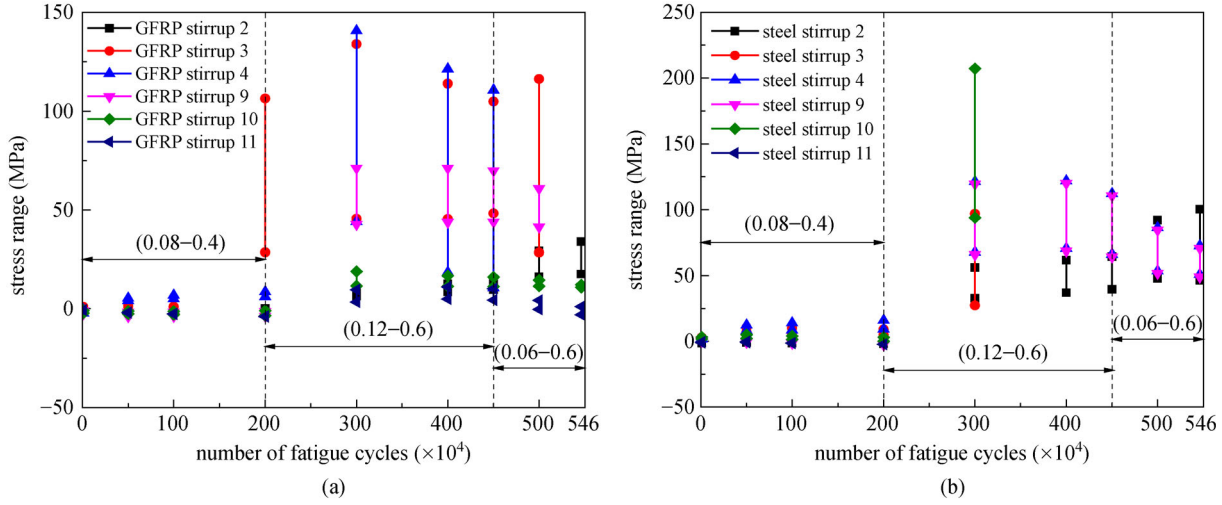

Fig. 11 Stress range in stirrups (FS-2.54-0.4): (a) Stress range in GFRP stirrups; (b) Stress range in steel stirrups.

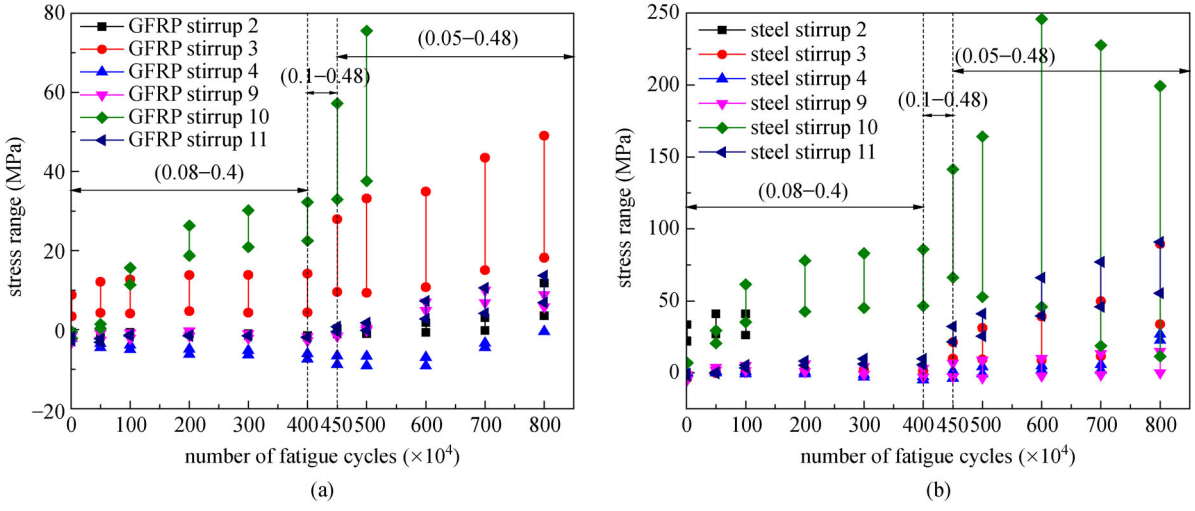

Fig. 12 Stress range in stirrups (FS-2.07-0.4): (a) stress range in GFRP stirrups; (b) stress range in steel stirrups.

the number of fatigue cycles. In addition, the stress ranges in the steel and GFRP stirrups were low before four million cycles, owing to the small stress level. From 4 to 4.5 million cycles, the maximum fatigue load increased, and thus the stress range in the stirrups increased. After 4.5 million cycles, the minimum fatigue load decreased, and thus the stress range in the stirrups increased. Comparing FS-2.54-0.4 and FS-2.07-0.4, the maximum and minimum stress levels were the same before two million cycles, and the only the shear span-to-depth ratio differed. As for FS-2.07-0.4, the stress range in the stirrups was larger, and the maximum crack width was larger.

3.4 Load-stirrup strain curves

The stirrup strain at the expected plane of shear failure (upper portion of vertical leg of #9 stirrups, middle of vertical leg of the #10 stirrups, lower portion of vertical leg of #11 stirrups) developed with the loading after different fatigue cycles, and the stirrup development in the middle of vertical leg of the #10 stirrup is shown in Fig. 13. When the load was less than 80 kN (about the cracking load), the stirrup strain showed small development as the load increased. After the cracking load, the stirrup strain increased significantly. Before four million cycles, the load-stirrup strain curves were approximately parallel, indicating that the residual strain in the stirrups increased with fatigue cycles. From 4 to 4.5 million cycles, the maximum fatigue load increased, and thus the residual strain in the stirrups increased more significantly.

3.5 Strain in longitudinal bars

3.5.1 Specimen FS-2.54-0.6

Figure 14 indicates that the strain in the longitudinal

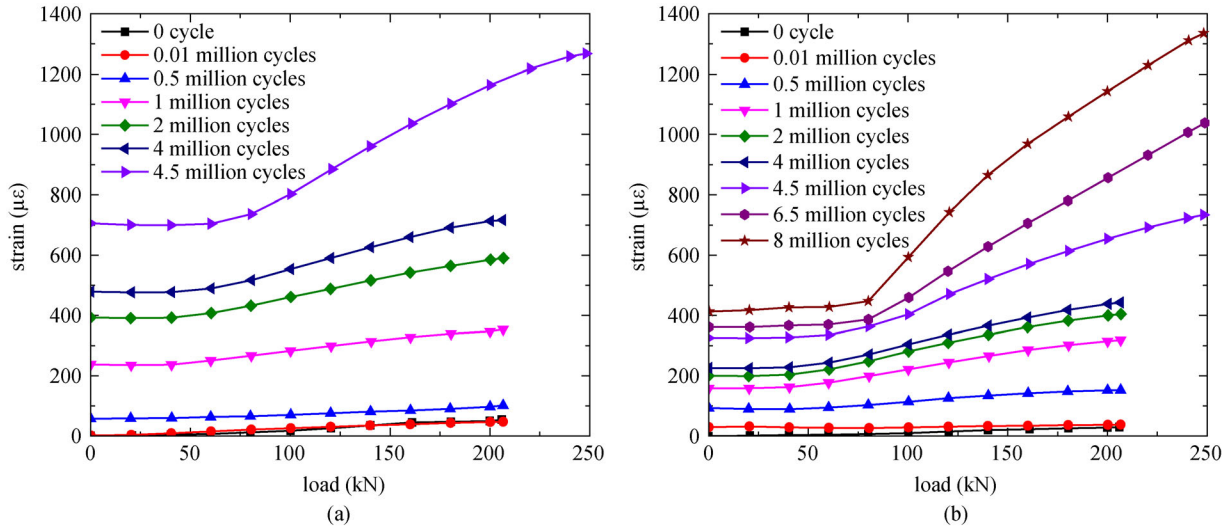

Fig. 13 Load-stirrup strain curves (FS-2.07-0.4): (a) middle of vertical leg of #10 GFRP stirrups; (b) middle of vertical leg of #10 steel stirrups.

tension bars developed with the fatigue cycles, and no steel bars yielded fatigue. Before 10000 cycles, the strain in the tension bars increased rapidly, and then the strain changed slightly with the fatigue cycles. The strain in the tension GFRP bar at mid-span, point *c* in Fig. 4(a), was larger than that of the steel bar, while the strain in the steel bar was larger in the shear span at points *b* and *d* in Fig. 4(a). At point *e*, the strain in the steel bar was larger than that of the GFRP bar before 50000 cycles, and it was surpassed by the strain in the GFRP bar after a significant increase in strain of the GFRP bar at 50000 cycles. Figure 7(b) shows that when the failure occurred at 400000 cycles, the strain in the tension steel and GFRP bars at point *e* decreased, while the strain in #11 steel and #11 GFRP stirrups, close to point *e*,

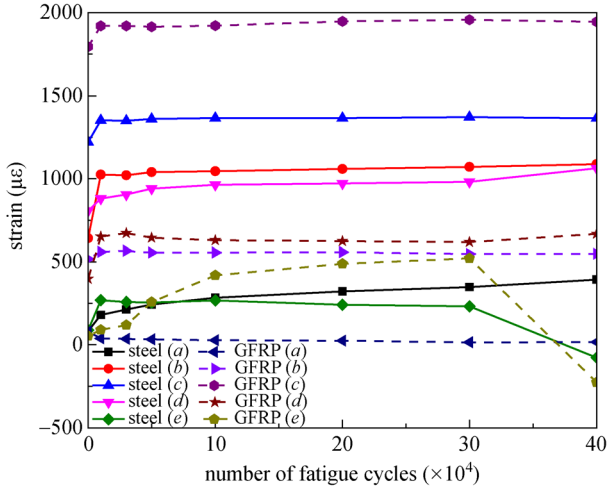

Fig. 14 Strain development in tension steel and GFRP bars with fatigue cycles under the upper limit of the fatigue load (FS-2.54-0.6).

increased significantly. This was owing to the stress redistribution.

3.5.2 Specimen FS-2.54-0.4

As presented in Fig. 15, the strain in the longitudinal tension bars developed with the fatigue cycles. The strain gauge at point *e* of the GFRP bar failed before the fatigue test. Before 10000 cycles, the strain in the tension bars increased rapidly, and then the strain changed slightly with the fatigue cycles as the upper and lower limits of the fatigue load remained unchanged. After two million cycles, the upper and lower limits of the fatigue load increased, and thus the strains in the tension steel and GFRP bars increased significantly. The strain in the tension steel bar at different locations was larger than that in the GFRP bar at the same location. One tension steel bar fractured at a location close to the #11 stirrups. According to Section 3.2.2, the #11 steel stirrup fractured at the lower bent portion after 4.7 million cycles, and more load was transferred to the tension bars, which may result in the fatigue fracture of the tension bars. After 4.9 million cycles, the strain in the tension GFRP bar increased dramatically to hundreds of thousands of micro-strain. Therefore, the tension steel bar may fracture at this time, which results in stress redistribution.

3.5.3 Specimen FS-2.07-0.4

Figure 16 shows that the strain in the longitudinal tension bars developed with the fatigue cycles, and no steel bars yielded in fatigue. Before 10000 cycles, the strain in the tension bars increased rapidly, and then the strain changed slightly with the fatigue cycles as the upper and lower

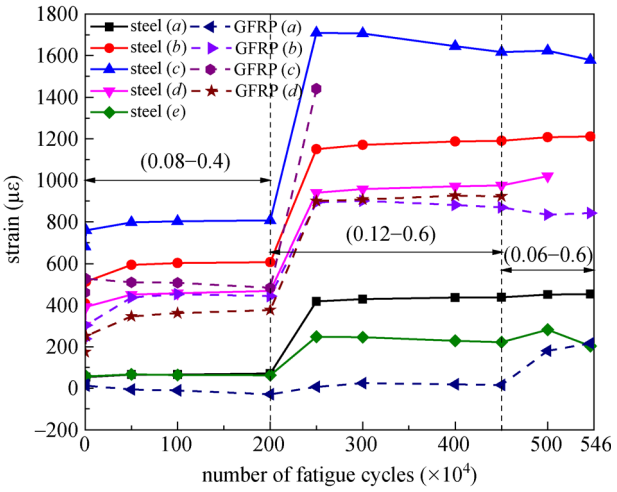

Fig. 15 Strain development in tension steel and GFRP bars with fatigue cycles under the upper limit of the fatigue load (FS-2.54-0.4).

limits of the fatigue load remained unchanged. After four million cycles, the upper and lower limits of the fatigue load increased, and thus the strains in the tension steel and GFRP bars increased significantly. The strain in the tension GFRP bar at mid-span, point *c* in Fig. 4(a), was larger than that in the steel bar, while the strain in the steel bar was larger in the shear span, points *b* and *d* in Fig. 4(a). At the support zone, points *a* and *e* in Fig. 4(a), there was hardly any difference between the strains of the steel and GFRP bars.

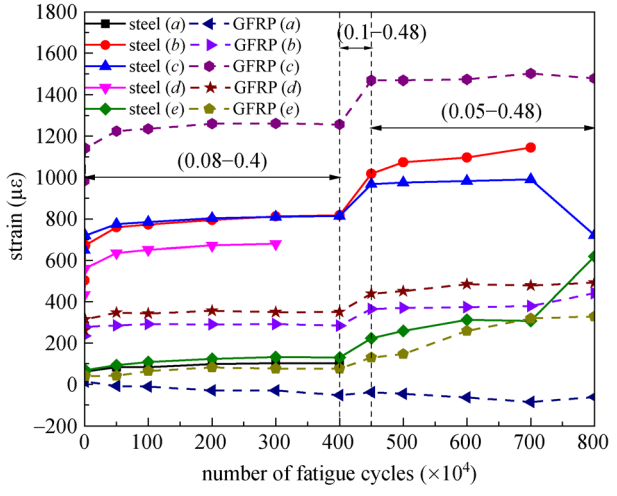

Fig. 16 Strain development in tension steel and GFRP bars with fatigue cycles under the upper limit of the fatigue load (FS-2.07-0.4).

Comparing Figs. 15 and 16, the difference between the strain in the tension bars of FS-2.54-0.4 and FS-2.07-0.4 was not large before two million cycles, except for the strain in the tension GFRP bar at mid-span (point *c*), which was different from the stirrup strain. This is because the stirrup strain is closely related to the crack development, whereas the strain in the tension bars is determined by the bending moment. Under the same upper limit of the fatigue load, the moment distributions of the two beams were similar, and thus the strain in the longitudinal bars was similar.

3.6 Mid-span deflection

The load–mid-span deflection curves are shown in Fig. 17. The slopes of the curves were reduced as cracks occurred during the static test before fatigue. The deflection increased as the number of fatigue cycles increased for all three specimens, particularly during the initial phase of fatigue, indicating the development of residual deflection. Stiffness degradation during fatigue was not statistically significant. For FS-2.54-0.4 and FS-2.07-0.4, the increase in the mid-span deflection was accelerated after the upper limit of the fatigue load increased. After the same number of fatigue cycles, the residual deflection of FS-2.54-0.6 was larger than that of FS-2.54-0.4, owing to the larger upper limit of the fatigue load for FS-2.54-0.6.

The load–mid-span deflection curves of FS-2.07-0.4 after eight million cycles are shown in Fig. 17(d). The specimen was loaded to 500 kN (the loading capacity of the system), unloaded, and then loaded again. The specimen failed at 491 kN, and the actual capacity was expected to be larger than 500 kN. Compared with the calculated static capacity of 523.3 kN, the capacity after fatigue had no significant decrease. For the first loading after eight million cycles, the slope of the rising section of the curve changed slightly, indicating that the stiffness of the beam changed to some extent. For the second loading, the slope of the rising section of the curve decreased, indicating that the stiffness of the beam was reduced.

3.7 Crack width

In the initial static test before fatigue loading, vertical cracks occurred at different locations along the beam, and inclined cracks developed near the loading zone. Figure 18 shows that the maximum widths of the diagonal cracks were measured under 0 kN and P_{max} in the initial and interim static tests. As for FS-2.54-0.6, the crack width increased significantly in the initial phase of fatigue (0–50000 cycles), and the rate of increase was lowered after 50000 cycles. For FS-2.54-0.4, the cracks developed slowly before two million cycles. After two million cycles, the crack width increased significantly owing to the increase in the upper limit of the fatigue load. Compared with FS-2.54-0.6, the stress level of FS-2.54-0.4 was smaller in the early phase of fatigue, it was adjusted to the same after two million cycles, and the load range of FS-2.54-0.4 increased again after 4.5 million. Eventually, the

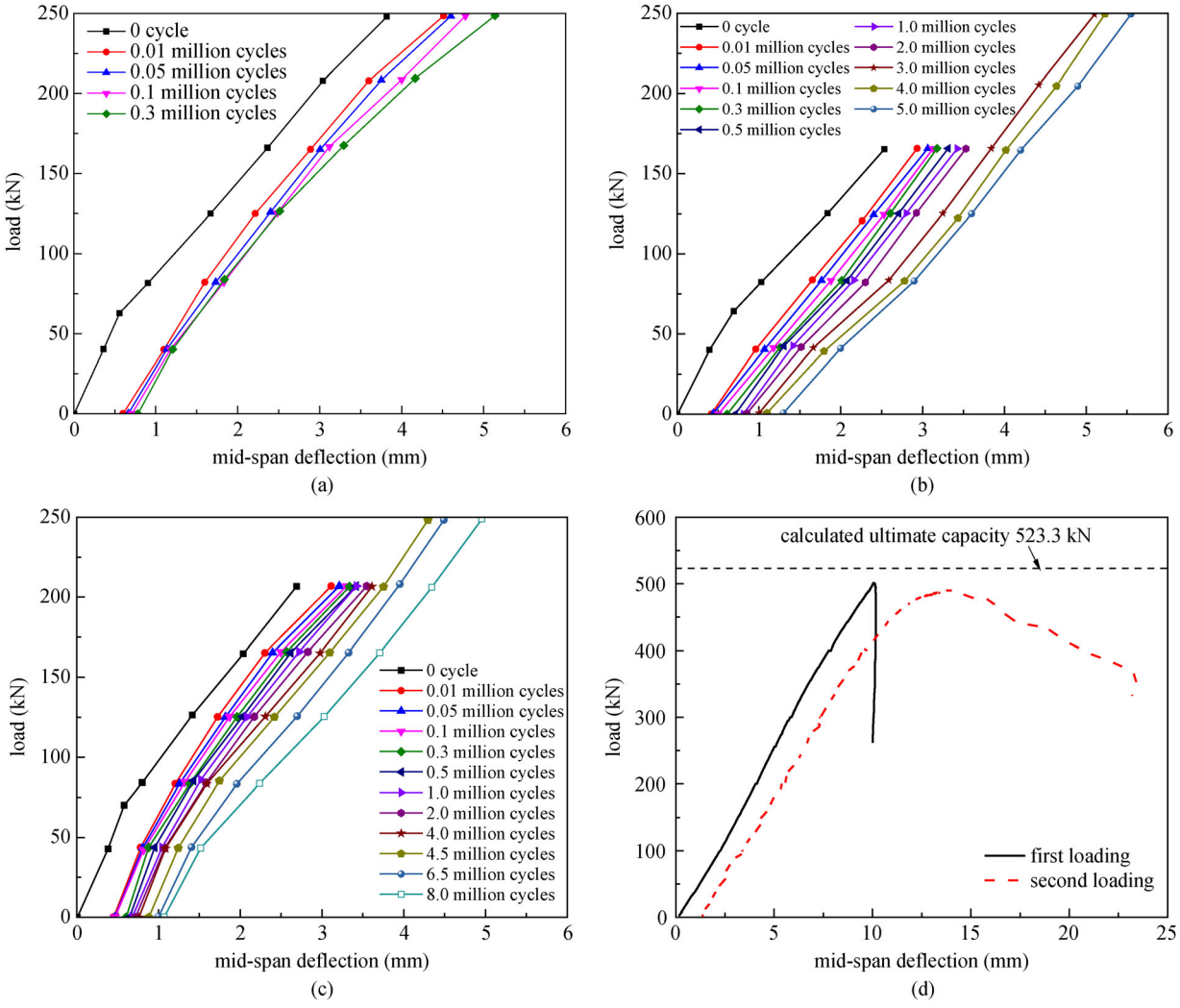

Fig. 17 Load–mid-span deflection curves for static tests after fatigue cycles: (a) FS-2.54-0.6; (b) FS-2.54-0.4; (c) FS-2.07-0.4; (d) FS-2.07-0.4 (after 8 million cycles).

crack width of FS-2.54-0.4 was still significantly smaller than that of FS-2.54-0.6. Therefore, the load level in the initial phase of fatigue has a greater influence on the crack development. As for FS-2.07-0.4, the maximum crack width did not change considerably before four million cycles, which was 0.2 mm under the upper limit of the fatigue load. It increased significantly with an increase in the upper limit of the fatigue load after four million cycles.

3.8 Fatigue life

The maximum stress ranges for the different reinforcements of the three specimens after one cycle and after the upper or lower limit of the fatigue load adjusted are listed in Table 4. The maximum stress range of the deformed steel bar can be determined using Eq. (4) according to ACI 215 R [31], where S_r is the stress range, in MPa or ksi, and its value is not less than 138 MPa (20 ksi); S_{min} is the algebraic minimum stress (positive value indicates tension, and negative value indicates compression) in MPa or ksi.

$$S_r = 161 - 0.33S_{min},\ (\text{MPa}) \tag{4a}$$

$$S_r = 23.4 - 0.33S_{min}.\ (\text{ksi}) \tag{4b}$$

AASHTO LRFD [34] presented a constant-amplitude fatigue threshold for straight reinforcement, as expressed in Eq. (5), where $(\Delta F)_{TH}$ is the constant-amplitude fatigue threshold, f_{min} is the minimum live-load stress, tension positive, compression negative, in ksi, and f_y is the specified minimum yield strength, and its value is not less than 60.0 ksi or greater than 100 ksi.

$$(\Delta F)_{TH} = 24 - 20f_{min}/f_y. \tag{5}$$

According to ACI 215R [31] and AASHTO LRFD [34], the stress thresholds for steel reinforcement were 138 and 165 MPa, respectively. The maximum stress range in the steel reinforcement of FS-2.54-0.6 was 175.5 MPa, which

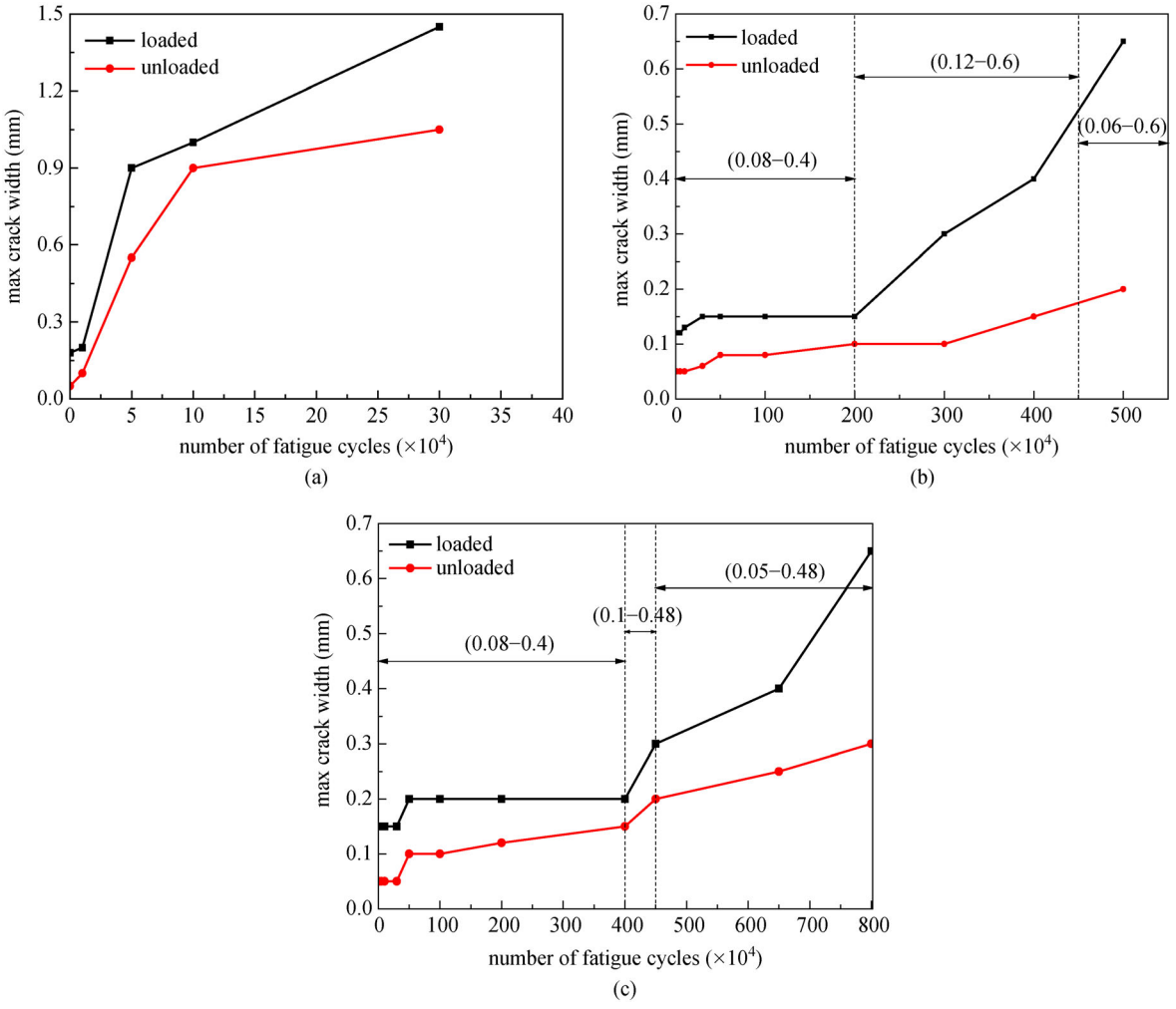

Fig. 18 Maximum crack width versus fatigue cycles: (a) FS-2.54-0.6; (b) FS-2.54-0.4; (c) FS-2.07-0.4.

was larger than 138 MPa and 165 MPa, the thresholds set by ACI 215R [31] and AASHTO LRFD [34], respectively. The specimen failed without fracture of any longitudinal steel bar at 405000 cycles. For FS-2.54-0.4, the maximum stress range in steel reinforcement increased from 97.9 to 220.3 MPa when the upper limit of the fatigue load increased after two million cycles, which was larger than aforementioned thresholds set by ACI 215R [31] and AASHTO LRFD [34]. One longitudinal steel bar fractured at 4.9 million cycles. The thresholds stipulated by the codes are conservative. As for FS-2.07-0.4, the maximum stress range in steel reinforcement increased from 85.0 to 118.2 MPa when the upper limit of the fatigue load increased after four million cycles, and to 133.9 MPa after 4.5 million cycles, which was less than the above-mentioned thresholds set by ACI 215R [31] and AASHTO LRFD [34]. In addition, no longitudinal steel bars fractured. The stress limit for GFRP reinforcement of the three specimens by ACI 440.1 R-15 [22] was $0.2 \times f_{fu}$, where f_{fu} is the design tensile strength of the GFRP bars. The threshold was not exceeded by any longitudinal GFRP bar.

For FS-2.54-0.6, the #10 GFRP stirrups fractured after 30000 cycles, the #10 steel stirrups fractured after 50000 cycles, and the beam failed after 405000 cycles. For FS-2.54-0.4, the #11 steel stirrup fractured after 4.7 million cycles, one steel bar fractured after 4.9 million cycles, and the beam failed after 5.46 million cycles. The fatigue failure of the specimens started with the fracture of the stirrups, and the specimens could last more fatigue cycles after one stirrup fractured. The fatigue strength of GFRP stirrups in the tests was considerably lower than that determined using axial tension tests on the GFRP bar in air and that found using beam-hinge tests on the GFRP bar, which were carried out by Noël and Soudki [33]. All the GFRP stirrups exhibited a clear fracture surface, not a typical broomlike failure in the fatigue tensile tests by Noël and Soudki [33]. This is because at the diagonal cracks, lateral shear developed in the stirrups, and the shear capacity of the GFRP reinforcement was low (150 MPa by

the manufacturer). GFRP stirrups were subjected to fatigue tension and shear, and failed owing to shear. In fatigue tests on I girders by Hanson et al. [35], it was found that lateral shear developed in the steel stirrups owing to diagonal cracks, which resulted in a decrease in the fatigue strength of steel stirrups. The fatigue loads for FS-2.54-0.4 and FS-2.54-0.6 were the same from 2 to 4.5 million cycles, which indicated that the initial fatigue level had a greater influence on the fatigue life.

4 Conclusions

The fatigue shear performance of hybrid RC beams was investigated through an experimental program, and the following conclusions were drawn.

1) The fatigue shear failure mode is summarized as follows: a critical diagonal crack was developed, all GFRP stirrups and some of the steel stirrups fractured at the critical diagonal crack, and the concrete at the top shear-compression zone was not crushed at failure.

2) Comparing the capacity from the static test after eight million cycles with the calculated static capacity, the fatigue cycling had no significant influence on the shear capacity.

3) The initial phase of fatigue and the upper limit of the fatigue load had a significant influence on the strain development in the longitudinal bars. The stress range in the steel and GFRP stirrups was closely related to the damage accumulation and fatigue life. The residual deflection increased with the fatigue cycles and the upper limit of the fatigue load. Fatigue had a small influence on the beam stiffness.

4) The fatigue strength of the GFRP stirrups in the tests was considerably lower than that of the axial tension test on the GFRP bar and that of the beam-hinge test on the GFRP bar. In addition, the failure mode was also different. Further studies are needed to investigate the stress distribution and failure criterion of GFRP stirrups under fatigue loading. Finite element analysis or other numerical analysis methods can be performed for further studies on this topic.

Acknowledgements The authors wish to acknowledge the research grants from the National Key Research and Development Program of China (2017YFC0703000) and the National Natural Science Foundation of China (Grant No. 51678430).

References

1. Arya C, Ofori-Darko F K, Pirathapan G. FRP rebars and the elimination of reinforcement corrosion in concrete structures. In: Taerwe L, ed. Proceedings of the Second International RILEM Symposium (FRPRCS-2). London: RILEM, E&FN Spon, 1995, 227–234
2. Aiello M A, Ombres L. Structural performances of concrete beams with hybrid (fiber-reinforced polymer-steel) reinforcements. Journal of Composites for Construction, 2002, 6(2): 133–140
3. Qu W J, Zhang X L, Huang H Q. Flexural behavior of concrete beams reinforced with hybrid (GFRP and steel) bars. Journal of Composites for Construction, 2009, 13(5): 350–359
4. El Refai A, Abed F, Al-Rahmani A. Structural performance and serviceability of concrete beams reinforced with hybrid (GFRP and steel) bars. Construction & Building Materials, 2015, 96: 518–529
5. Newhook J P. Design of under-reinforced concrete T-sections with GFRP reinforcement. In: Humar J, Razaqpur A G, eds. Proceedings of the 3rd International Conference on Advanced Composite Materials in Bridges and Structures. Montreal: Canadian Society for Civil Engineering, 2000, 153–160
6. Lau D, Pam H J. Experimental study of hybrid FRP reinforced concrete beams. Engineering Structures, 2010, 32(12): 3857–3865
7. Pang L, Qu W J, Zhu P, Xu J J. Design propositions for hybrid FRP-steel reinforced concrete beams. Journal of Composites for Construction, 2016, 20(4): 04015086
8. Kara I F, Ashour A F, Köroğlu M A. Flexural behavior of hybrid FRP/steel reinforced concrete beams. Composite Structures, 2015, 129: 111–121
9. Bencardino F, Condello A, Ombres L. Numerical and analytical modeling of concrete beams with steel, FRP and hybrid FRP-steel reinforcements. Composite Structures, 2016, 140: 53–65
10. Zhu P, Xu J J, Qu W J, Hao H. Experimental study of fatigue flexural performance of concrete beams reinforced with hybrid GFRP and steel bars. Journal of Composites for Construction, 2017, 21(5): 04017036
11. Xu J J, Zhu P, Ma Z J, Qu W J. Fatigue flexural analysis of concrete beams reinforced with hybrid GFRP and steel bars. Engineering Structures, 2019, 199: 109635
12. Li L J, Hou B, Lu Z Y, Liu F. Fatigue behaviour of sea sand concrete beams reinforced with basalt fibre-reinforced polymer bars. Construction & Building Materials, 2018, 179: 160–171
13. Zhao J, Li G H, Wang Z K, Zhao X L. Fatigue behavior of concrete beams reinforced with glass- and carbon-fiber reinforced polymer (GFRP/CFRP) bars after exposure to elevated temperatures. Composite Structures, 2019, 229: 111427
14. Zhang X L. Flexural and shear behavior of concrete beams reinforced with hybrid (FRP and steel) bars. Dissertation for the Doctoral Degree. Shanghai: Tongji University, 2010 (in Chinese)
15. Pang L. Investigation of concrete members reinforced with steel and FRP bars for sectional equal durability. Dissertation for the Doctoral Degree. Shanghai: Tongji University, 2016 (in Chinese)
16. Ruhnau J. Influence of repeated loading on the stirrup stress of reinforced concrete beams. ACI Special Publications, 1974, 42(7): 169–181
17. Okamura H, Farghaly S A, Ueda T. Behaviors of reinforced concrete beams with stirrups failing in shear under fatigue loading. In: Proceedings of the Japan Society of Civil Engineers. Tokyo: Japan Society of Civil Engineers, 1981, 109–122
18. Ueda T. Behavior in shear of reinforced concrete beams under fatigue loading. Dissertation for the Doctoral Degree. Tokyo: University of Tokyo, 1982
19. Kwak K H, Park J G. Shear-fatigue behavior of high-strength reinforced concrete beams under repeated loading. Structural

Engineering and Mechanics, 2001, 11(3): 301–314
20. Teng S, Ma W, Wang F. Shear strength of concrete deep beams under fatigue loading. ACI Structural Journal, 2000, 97(4): 572–580
21. Isojeh B, El-Zeghayar M, Vecchio F J. High-cycle fatigue life prediction of reinforced concrete deep beams. Engineering Structures, 2017, 150: 12–24
22. ACI 440.1R–15. Guide For The Design And Construction of Structural Concrete Reinforced With FRP Bars. Farmington Hills: American Concrete Institute, 2015
23. GB/T 228.1–2010. Metallic Materials-Tensile Testing-Part 1: Method of Test at Room Temperature. Beijing: General Administration of Quality Supervision, Inspection and Quarantine of the People's Republic of China, 2010
24. GB/T 30022–2013. Test Method For Basic Mechanical Properties Of Fiber Reinforced Polymer Bar. Beijing: General Administration of Quality Supervision, Inspection and Quarantine of the People's Republic of China, 2013
25. GB/T 50081–2002. Standard for Test Method of Mechanical Properties on Ordinary Concrete. Beijing: China Building Industry Press, 2002
26. ACI Committee 318–14. Building Code Requirements for Structural Concrete and Commentary. Farmington Hills: American Concrete Institute, 2014
27. Bischoff P H. Reevaluation of deflection prediction for concrete beams reinforced with steel and fiber reinforced polymer bars. Journal of Structural Engineering, 2005, 131(5): 752–767
28. Alsayed S H, Al-Salloum Y A, Almusallam T H. Performance of glass fiber reinforced plastic bars as a reinforcing material for concrete structures. Composites. Part B, Engineering, 2000, 31(6–7): 555–567
29. Rafi M M, Nadjai A, Ali F, Talamona D. Aspects of behaviour of CFRP reinforced concrete beams in bending. Construction & Building Materials, 2008, 22(3): 277–285
30. Zhang J, Stang H, Li V C. Fatigue life prediction of fiber reinforced concrete under flexural load. International Journal of Fatigue, 1999, 21(10): 1033–1049
31. ACI Committee 215. Considerations for design of concrete structures subjected to fatigue loading. ACI 215R–74 (Revised 1992/ Reapproved 1997). Farmington Hills: American Concrete Institute, 1997
32. Heffernan P J, Erki M A. Fatigue behavior of reinforced concrete beams strengthened with carbon fiber reinforced plastic laminates. Journal of Composites for Construction, 2004, 8(2): 132–140
33. Noël M, Soudki K. Fatigue behaviour of GFRP reinforcing bars in air and in concrete. Journal of Composites for Construction, 2014, 18(5): 04014006
34. AASHTO Committee. AASHTO LRFD Bridge Design Specifications. 7th ed. Washington, DC: American Association of State Highway and Transportation Officials, 2014
35. Hanson J M, Hulsbos C L, VanHorn D A. Fatigue tests of prestressed concrete I-beams. Journal of the Structural Division, 1970, 96(11): 2443–2464